Available online at www.sciencedirect.com
SCIENCE DIRECT®
Journal of Crystal Growth 277 (2005) 192–199
JOURNAL OF CRYSTAL GROWTH
www.elsevier.com/locate/jcrysgro

Efficient UV photoluminescence from monodispersed secondary ZnO colloidal spheres synthesized by sol–gel method

Hsin-Ming Cheng[a,b,*], Hsu-Cheng Hsu[a], Shiow-Lian Chen[b], Wen-Ti Wu[b], Chih-Chun Kao[b], Li-Jiaun Lin[b], Wen-Feng Hsieh[a,1]

[a]*Department of Photonics and Institute of Electro-Optical Engineering, National Chiao Tung University, 1001 Tahsueh Rd., Hsinchu 30050, Taiwan*

[b]*Materials Research Laboratories, Industrial Technology Research Institute, Bldg. 77, 195 Section 4 Chung Hsing Road, Chutung, Hsinchu 310, Taiwan, Republic of China*

Received 8 October 2004; accepted 23 December 2004
Communicated by M. Schieber
Available online 29 January 2005

Abstract

ZnO colloidal spheres were synthesized by sol–gel method with a narrow size distribution. We controlled the size of the spheres during the secondary reaction with various amounts of primary reaction supernatant. The optimized condition of ZnO powders with an average diameter of 185 nm was obtained for structure analysis and study of optical properties. Transmission electron microscopy and X-ray diffraction reveal that the spheres are polycrystalline in the pure wurtzite phase. Markedly enhanced near-band-edge ultraviolet photoluminescence and significantly reduced defect-related visible emission were also observed. We attribute this observation to the localized bound excitons with high density of defect states. In addition, broad yellow emission and green emission were observed when the powders were post-annealed at 500 °C in air ambience. The origins of the defect-induced visible emissions are attributed to oxygen interstitials and oxygen vacancies.

PACS: 78.67.Bf; 81.07.Wx; 81.20.Fw

Keywords: A1. photoluminescence; A3. Sol–gel; B1. nanomaterials; B1. ZnO

1. Introduction

ZnO is a versatile material and has been found to meet wide applications in the fields of electronics [1,2], optoelectronics [3], and gas sensing [4–6]. As a wide band gap semiconductor, ZnO has achievable

*Corresponding author. Department of Photonics and Institute of Electro-Optical Engineering, National Chiao Tung University, 1001 Tahsueh Rd., Hsinchu 30050, Taiwan. Tel.: +886 3 5712121x56316; fax: +886 3 5716631.
E-mail addresses: smcheng@itri.org.tw (H.-M. Cheng), wfhsieh@mail.nctu.edu.tw (W.-F. Hsieh).
[1]Also for correspondence.

0022-0248/$ - see front matter © 2005 Elsevier B.V. All rights reserved.
doi:10.1016/j.jcrysgro.2004.12.133

applications as a transparent electrode [7,8] for photovoltaic and electroluminescent devices and as a promising material for ultraviolet light emitting devices and laser diodes [9,10]. Furthermore, luminescence of ZnO phosphors has recently regained much interest because of its potential use in low-voltage fluorescence. Especially, since ZnO has a direct band gap of 3.37 eV at room temperature, high mechanical and thermal stabilities, and much larger free exciton binding energy (60 meV) than that of GaN (25 meV), it ensures an efficient excitonic emission up to room temperature.

Accordingly, the preparation of uniform property about ZnO powders has attracted much attention in order to possess stable luminescent properties. Different methods such as precipitation [11,12], spray pyrolysis[13,14], microemulsion [15,16], hydrothermal synthesis [17,18] and sol–gel process [19,20] have been utilized for preparing ZnO powder. Among these methods the sol–gel process is a relatively simple one for preparation of ZnO nanoparticles. It allows the production of ZnO colloids with narrow size distribution and excellent crystallization. However, the characteristics of electronic and luminescence are markedly influenced by the experimental parameters used in the sol–gel method such as the precursor, solvent, heating temperature and so on.

In the present work, sol–gel method was used to synthesize monodisperse ZnO colloidal spheres. The ZnO colloidal spheres appear to be formed by the aggregation of very small primary crystallites and those secondray clusters were investigated to have the random lasing effect [20]. However, the influences of luminescence on the primary particles were not discussed before. We demonstrated the high-efficient ultraviolet (UV) emission of the primary single crystallites by measuring room-temperature (RT) and low-temperature (LT) photoluminescence (PL). The synthesis mechanism and crystal structure of the ZnO colloidal spheres are also discussed.

2. Experiments

The ZnO colloidal spheres were produced by a two-stage reaction process similar to that described by Seelig et al. [21], and reactions were ascribed as the following equations:

$$\mathrm{Zn(CH_3COO)_2} + x\mathrm{H_2O} \xrightarrow{\Delta} \mathrm{Zn(OH^-)}_x (\mathrm{CH_3COO^-})_{2-x} + x\mathrm{CH_3COOH}, \quad (1)$$

$$\mathrm{Zn(OH^-)}_x(\mathrm{CH_3COO^-})_{2-x} \xrightarrow{\Delta} \mathrm{ZnO} + (x-1)\mathrm{H_2O} + (2-x)\mathrm{CH_3COOH}. \quad (2)$$

Eq. (1) is the hydrolysis reaction for $Zn(OAc)_2$ to form metal complexes. We increased the temperature of reflux from RT to 160 °C and maintained for aging. The zinc complexes would dehydrate and remove acetic acid to form pure ZnO as Eq. (2) during the aging time. Actually, these two reactions described above proceed simultaneously while the temperature is over 110 °C. All chemicals used in this study were reagent grade and employed without further purification. In a typical reaction, 0.01 mol zinc acetate dehydrate (99.5% $Zn(OAc)_2$, Riedel-deHaen) was added to 100 ml diethylene glycol (99.5% DEG, EDTA). Then the temperature of reaction solution was increased to 160 °C and maintained for aging at least for 1 h. White colloidal ZnO was formed in the solution that was employed as the primary solution. The secondary solution was composed of $Zn(OAc)_2$ (0.01 mol) and various amounts of primary supernatant (5–20 ml) in 100 ml DEG and the reaction began in the same way as the primary reaction. The white gelatinous production of ZnO particles ranging in diameter from 50 to 300 nm (depending on the amount of primary supernatant [21]) were successfully synthesized under the well-controlled concentration with stable heating rate. From our observations, the particles with a diameter of nearly 185 nm have the optimal size that can be used to fabricate self-assembled periodic array; we therefore choose the ZnO colloidal spheres with size lying in 185 nm to study their structural and optical properties throughout this report. The powder specimens were prepared by placing a drop of colloidal suspension on preheated Si(1 0 0) substrates and carbon-coated copper grids and were then allowed to dry in air to remove the excess solvent. Finally, the dry powders were inserted in a furnace and heated at 350 °C and 500 °C for 1 h in air ambience.

The crystalline structure of the samples was analyzed by using Philips PW1700 X-ray diffractometer (XRD) with Cu Kα radiation and JEOL JEM-2000FX transmission electron microscope (TEM) operated at 200 keV. The morphology and size distribution were characterized using a LEO-1530 field emission scanning electron microscope (FE-SEM) operated at 5 keV. The composition of specimens was analyzed using an EDAX energy-dispersive X-ray (EDX) spectrometer attached to the SEM. The Raman spectroscopy was performed using an Ar-ion laser with 488 nm wavelength and 150 mW power as the excitation source. The scattered light was collected in the back-scattering geometry and detected by the SPEX-1877 triplemate equipped with liquid nitrogen cooled CCD. The photoluminescence measurement was made using a 20 mW He-Cd laser at wavelength of 325 nm and the emission light was dispersed by a TRIAX-320 spectrometer and detected by a UV-sensitive photomultiplier tube. A closed cycle refrigerator was used to maintain the measured temperature at 10 K.

3. Results and discussion

The SEM photographs shown in Fig. 1 are the products synthesized in various aging times using 10 ml of primary supernatant. ZnO was agglomerated from the beginning as white seeds shown in Fig. 1(a). The zinc complexes link as networks initially [see Fig. 1(b)] and condensed isotropic to finally form hierarchical packing of colloidal particles as shown in Fig. 1(c). The unidirectional aggregate phenomenon and formation mechanism were presented by Ocana et al. [22] in other metal oxide colloidal systems. The monodispersed spherical ZnO colloids with an average particle size of ca. 185 nm were obtained after at least one hour aging. Careful analysis of the micrographs determines that the spheres formed are monodispersive within 5–10%. The EDX spectra of the products with different aging times in Fig. 2 reveal that they contain Zn, O and C. The carbon proportion decreases as the aging time increases. This means that it is necessary for the products to have enough aging time to remove ethanoate ion.

Fig. 3 shows TEM micrograph of the above investigated samples. A spherical shape of the ZnO clusters is recognized at about 185 nm with agglomeration of primary single crystallites ranging from 6 to 12 nm. Electron diffraction pattern confirms the polycrystalline structure of the secondary colloidal ZnO spheres that were aggregated of the primary single crystallites.

Crystal structure of the ZnO spheres was analyzed by using a powder XRD as shown in

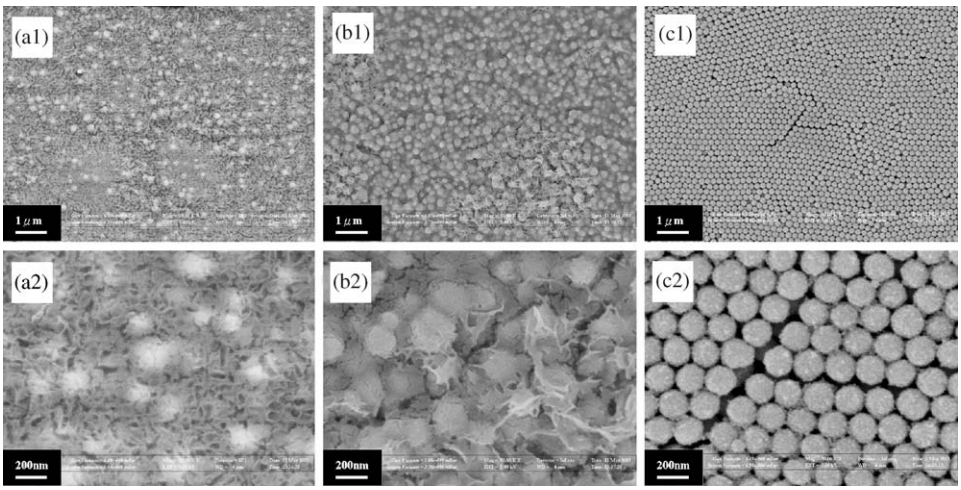

Fig. 1. Large and local scale of scanning electron micrographs of various aging time products synthesized using 10 ml of primary supernatant. The aging times are (a) 15 min, (b) 30 min and (c) 60 min.

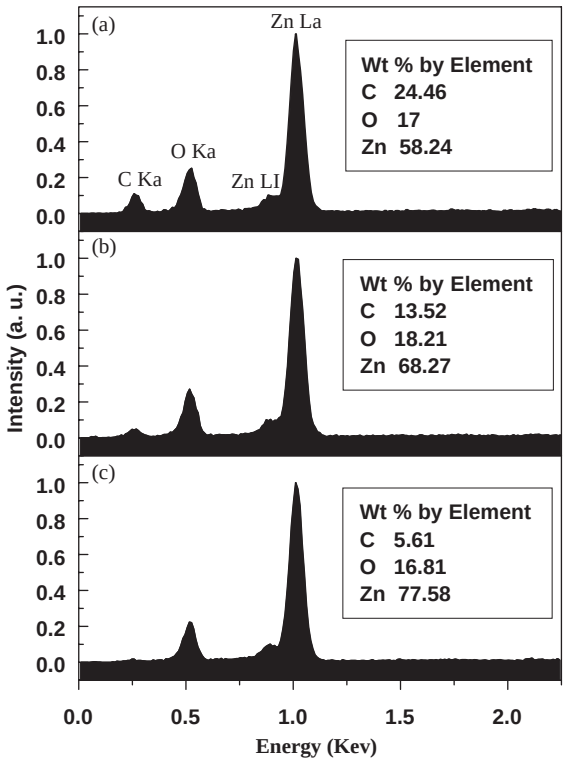

Fig. 2. Composition variation analysis by energy dispersive X-ray spectra of different aging time products as (a) 15 min, (b) 30 min and (c) 60 min.

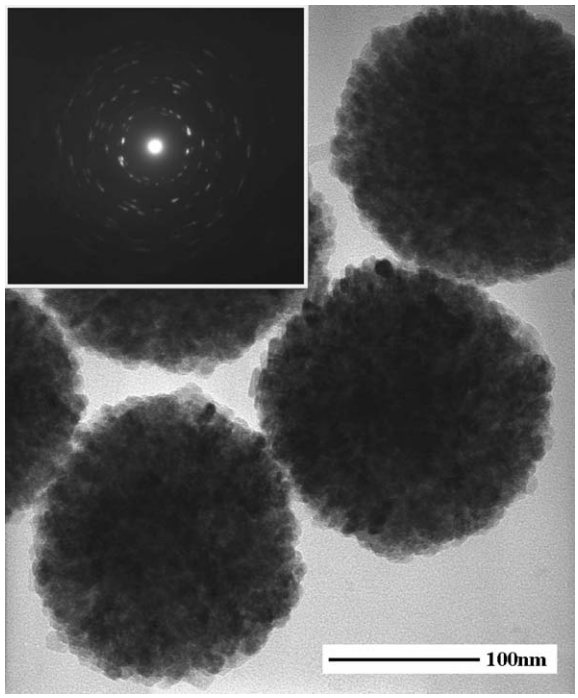

Fig. 3. Transmission electron micrograph and selected area diffraction pattern of the secondary ZnO clusters.

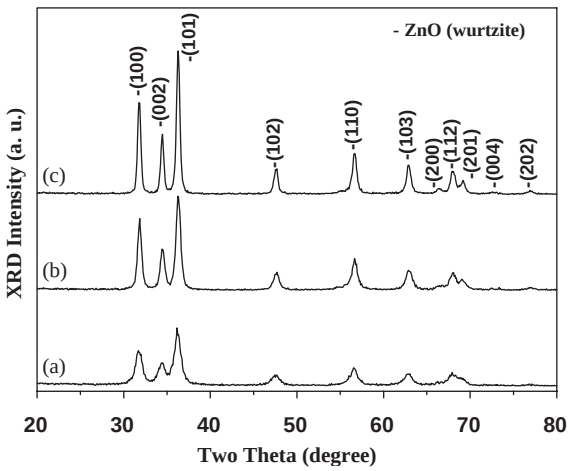

Fig. 4. X-ray diffraction patterns of (a) as-grown, (b) 350 °C annealing for 1 h and (c) 500 °C annealing for 1 h polycrystalline ZnO colloidal spheres.

Fig. 4. We demonstrated the XRD profiles of the as-grown powders and the samples post-annealed at 350 °C and 500 °C in air ambience for 1-h, respectively. The diffraction peaks and their relative intensities coincide with the JCPDS card no. 36-1451, so that the observed patterns can be unambiguously attributed to the presence of hexagonal wurzite crystallites. Diffraction fingerprints can also be indexed to a structure of polycrystalline ZnO with cell constants of $a = 3.251$ Å and $c = 5.208$ Å. Furthermore, the crystalline sizes were approximately estimated to be 9, 14, and 20 nm for as-grown, 350 °C-annealed and 500 °C-annealed samples, respectively, by using the Scherrer equation from the full-width at half-maximum (FWHM) of diffraction peaks by considering instrumental broadening effect. The result was directly implied the grain growth of the ZnO colloidal spheres under heat treatment.

To investigate the relationship of the crystalline quality, Raman spectra were also measured for ZnO spheres before and after heat treated under

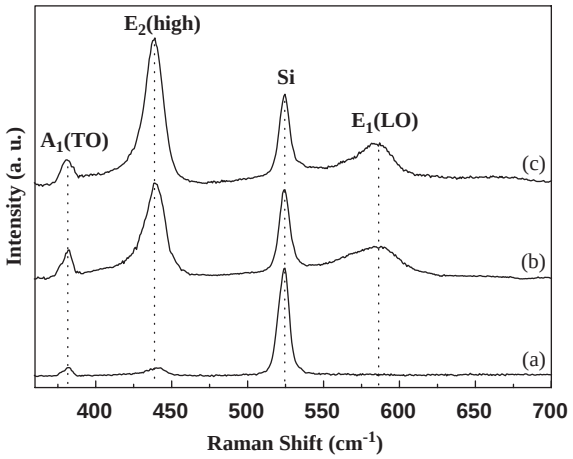

Fig. 5. Raman spectra of (a) as-grown, (b) 350 °C annealing for 1 h and (c) 500 °C annealing for 1 h ZnO colloidal spheres.

various temperatures. Fig. 5 presents the spectra of the as-grown powders, and after 350 °C annealing and 500 °C annealing for 1 h, respectively. The dominant feature at ~520 cm^{-1} is due to the TO phonon mode from the Si substrate. The peak at 380 cm^{-1} corresponds to A_1(TO) phonon of ZnO crystal, while the peak at 437 cm^{-1} corresponds to E_2(high) mode of ZnO crystal [23]. We found that there is no significant change of Raman spectra for the 350 °C-annealed and 500 °C-annealed samples. Consequently, after thermal annealing over 350 °C, the E_2(high) mode became sharper and stronger and another E_1(LO) mode was observed at 580 cm^{-1}. A stronger E_2(high) mode means good crystallinity. Whereas, the observance of E_1(LO) mode is associated with existence of the oxygen vacancy, interstitial zinc, or their complexes [24–26].

The room-temperature (RT) PL of the ZnO spheres with different calcination temperatures is shown in Fig. 6. For the as-grown ZnO spheres [Fig. 6(a)], the spectrum consists of a strong UV band emission, located at 3.3 eV with the FWHM 160 meV, and there are relatively by no other visible emissions. The UV emission is attributed to excitonic recombination [27]. After post-annealing in air ambience [Fig. 6(b) 350 °C and Fig. 6(c) 500 °C], the UV band emission was slightly red shifted to 3.2 eV with reduced intensity and

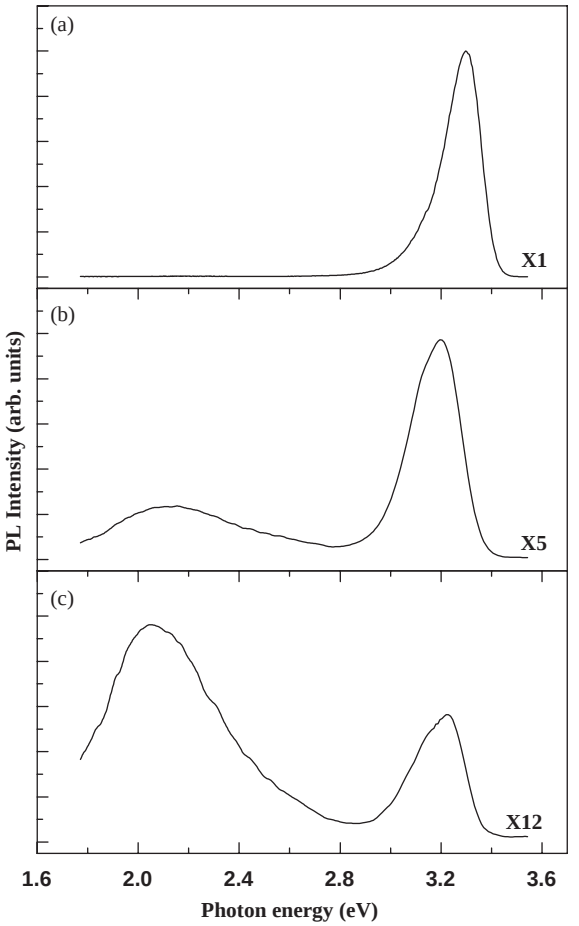

Fig. 6. Room-temperature photoluminescence spectra of (a) as-grown, (b) 350 °C annealing for 1 h and (c) 500 °C annealing for 1 h ZnO powders.

broadened FWHM, while the broad visible band emission at local maximum 2.1 eV was enhanced with increasing annealing temperature. Fig. 7 shows the low temperature (LT) PL spectra of the same samples measured at 10 K. The LTPL indicates that the UV band emission is still broad for the as-grown ZnO spheres [Fig. 7(a)] and the peak position located at 3.37 eV with FWHM of 130 meV. As the annealing temperature is increased [Fig. 7(b) 350 °C and Fig. 7(c) 500 °C], the FWHM of UV peaks becomes narrower especially for the 500 °C-annealed sample. This is due to grain growth at high annealing temperature and is also confirmed by the peaks width of XRD

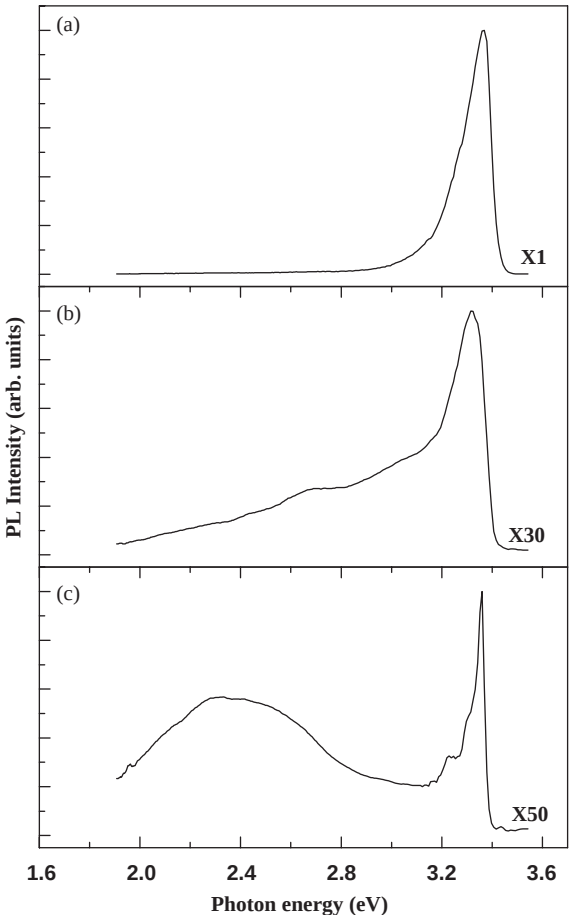

Fig. 7. Low-temperature (10 K) photoluminescence spectra of (a) as-grown, (b) 350 °C annealing for 1 h and (c) 500 °C annealing for 1hour ZnO powders.

in Fig. 4. The donor-bound exciton (D°X) peak situated at 3.37 eV of Fig. 7(c) is predominant with its longitudinal (LO) phonon replicas at the lower energy side, which is similar to the bulk crystal for the annealed temperature at 500 °C.

With comparison of the RTPL studies, the temperature dependences of the peak shifts for as-grown and 500 °C-annealed powders in Fig. 6(a) and (c) and Fig. 7(a) and (c) were obvious. The differences of the peak energy between bulk ZnO and both of the as-grown and the 500 °C-annealed powders were 0.07 and 0.14 eV, respectively. Since the annealed 500 °C powders present the bulk property and the donor-bound exciton was reported as temperature dependent exciton luminescent energy [28], the broadening UV emission of as-grown powders must come from another physical mechanism. Yang et al. [27] have proposed that bound to deep centers (localized states) exist in the ZnO quantum dots. The emission peak of the bound excitons hardly changes with temperature and presents broad LTPL spectrum. Furthermore, those defect-bound excitons have a large density of states, so they probably enhance the emission intensity of UV luminescence. The UV emission at 3.3 eV of the as-grown powders of our work may also be due to the defect-related levels but do not come from free exciton.

It is generally agreed that the visible emission is due to nonstoichiometric composition and visible photoluminescence is most commonly green [29–32], though other peaks are, for example, yellow [33–35] and orange emission [36]. In our RTPL spectra, the broad yellow emission at local maximum position 2.1 eV was observed when we increased annealing temperature from 350 °C to 500 °C. The deep level involved in the yellow luminescence of ZnO is attributed to oxygen interstitials (O_i) [33,35]. The origin is due to oxygen diffusion of the ZnO spheres after annealing in air atmosphere and is also consistent with the previous study for ZnO samples sintered in moist air [33]. Furthermore, Greene et al. [34] have also provided the strong evidence of disappearance of the yellow emission in oxygen-deficient ZnO nanowires after annealing in reducing atmosphere. Consequently, the yellow emission in our present work is associated with oxygen interstitials (O_i) beyond all doubt.

However, LTPL spectra shown in Fig. 7 depict the broad visible emission of the 500 °C-annealed powders at around 2.3 eV (green emission) in low temperature. The green emission may come from oxygen vacancies (V_o) as the previous reports indicate [29–32], and the results also agree with the previous discussion on Raman spectra. The possible reason is the suppression of yellow luminescence while green emission remained because of their different activation energies. Due to the activation energy of O_i induced excitation was 71 meV[Ref. [34]; yellow emission can be seen at room temperature readily. The binding energy of

green emission could be smaller than thermal energy at room temperature (25 meV) and result in hardly appearing at RT in our case. Although no evidence of the suggestion we described above is appropriate, the origin of the visible emissions in ZnO is a controversial one. The other analytical methods such as electron paramagnetic resonance (EPR) and temperature-dependent photoluminescence can be used to confirm this controversy in our further investigation.

4. Conclusion

In summary, we have successfully demonstrated the monodispersed secondary ZnO colloidal spheres synthesized by a simple sol–gel method and the influence of aging time on the density of powders was presented confidently. Transmission electron micrograph shows ZnO clusters were aggregated of primary single crystallites with a size of 6–12 nm. Higher efficient near band edge UV luminescence was attributed to defect-bound excitons with high density of states and we confirm it by using room-temperature and low-temperature photoluminescence analyses. The assumption was proved from the observation of peak broadening and unchanged position in low-temperature photoluminescent spectra. The interesting features are similar to the behavior of ZnO quantum dots in the previous study. In addition, broad yellow emission and green emission were observed in RTPL and LTPL, respectively. The defects such as oxygen interstitials (O_i) and oxygen vacancies (V_o) dominate the visible emissions of ZnO spheres in temperature-dependent photoluminescence.

Acknowledgements

We would like to gratefully acknowledge financial support from the National Science Council (NSC) in Taiwan under Contract No. NSC-93-9112-M-009-035. One of authors (H. C. Hsu) acknowledges NSC for providing a fellowship. We also thank the TEM group of MRL/ITRI for the help on electron microscopy measurements.

References

[1] M.S. Ramanchalam, A. Rohatgi, W.B. Carter, J.P. Shaffer, T.K. Gupta, J. Electron Mater. 24 (1995) 413.
[2] W.-C. Shin, M.-S. Wu, J. Crystal Growth 137 (1994) 319.
[3] H. Nanto, T. Minami, S. Takata, Phys. Status Solidi A 65 (1981) K131.
[4] F.C. Lin, Y. Takao, Y. Shimizu, M. Egashira, Sensor. Actuator. B 24–25 (1995) 843.
[5] K.S. Weissenrieder, J. Muller, Thin Solid Films 30 (1997) 300.
[6] J. Muller, S. Weissenrieder, J. Anal. Chem. 349 (1994) 380.
[7] Karin. Keis, Nanostructured ZnO Electrodes for Solar Cell Applications, Acta Universitatis Upsaliensis, Uppsala, 2001.
[8] R.L. Hoffman, B.J. Norris, J.F. Wagera, Appl. Phys. Lett. 82 (2003) 733.
[9] Z.K. Tang, G.K.L. Wong, P. Yu, M. Kawasaki, A. Ohtomo, H. Koinuma, Y. Segawa, Appl. Phys. Lett. 72 (1998) 3270.
[10] T. Makino, C. Chia, Y. Segawa, M. Kawasaki, A. Ohtomo, K. Tamura, Y. Matsumoto, H. Koinuma, Appl. Surf. Sci. 189 (2002) 277.
[11] M.E.V. Costa, J.L. Baptista, J. Eur. Ceram. Soc. 11 (1993) 275.
[12] S.M. Haile, D.W. Johnson, G.H. Wiseman, H.K. Bowen, J. Am. Ceram. Soc. 72 (1989) 2004.
[13] O. Milosevic, B. Jordovic, D. Uskokovic, Mater. Lett. 19 (1994) 165.
[14] K. Vanheusden, C.H. Seager, W.L. Warren, D.R. Tallant, J. Caruso, M.J. Hampden-Smith, T.T. Kodas, J. Lumin. 75 (1997) 11.
[15] M. Singhal, V. Chhabra, P. Kang, D.O. Shah, Mater. Res. Bull. 32 (1997) 239.
[16] B.P. Lim, J. Wang, S.C. Ng, C.H. Chew, L.M. Gan, Ceram. Int. 24 (1998) 205.
[17] C.-H. Lu, C.-H. Yeh, Mater. Lett. 33 (1997) 129.
[18] A. Chittofrati, E. Matijević, Colloids Surf 48 (1990) 65.
[19] L. Spanhel, M. Anderson, J. Am. Chem. Soc. 113 (1991) 2826.
[20] H. Cao, J.Y. Xu, E.W. Seelig, R.P.H. Chang, Appl. Phys. Lett. 76 (2000) 2997.
[21] E.W. Seelig, B. Tang, A. Yamilov, H. Cao, R.P.H. Chang, Mater. Chem. Phys. 80 (2003) 257.
[22] M. Ocana, R. Clemente, C.J. Serna, Adv. Mater. 7 (1995) 212.
[23] T.C. Damen, S.P.S. Porto, B. Tell, Phys. Rev. 142 (1966) 570.
[24] G.J. Exarhos, S.K. Sharma, Thin Solid Films 270 (1995) 27.
[25] X.L. Xu, S.P. Lau, J.S. Chen, G.Y. Che, B.K. Tay, J. Crystal Growth 223 (2001) 201.
[26] N. Ashkenov, B.N. Mbenkum, C. Bundesmann, V. Riede, M. Lorenz, D. Spemann, E.M. Kaidashev, A. Kasic, M. Schubert, M. Grundmann, G. Wagner, H. Neumann, V. Darakchieva, H. Arwin, B. Monemar, J. Appl. Phys. 93 (2003) 126.

[27] C.L. Yang, J.N. Wang, W.K. Ge, L. Guo, S.H. Yang, D.Z. Shen, J. Appl. Phys. 90 (2001) 4983.
[28] D.W. Hamby, D.A. Lucca, M.J. Klopfstein, G. Cantwell, J. Appl. Phys. 93 (2003) 3214.
[29] K. Vanheusden, C.H. Seager, W.L. Warren, D.R. Tallant, J.A. Voigt, Appl. Phys. Lett. 68 (1998) 403.
[30] K. Vanheusden, W.L. Warren, C.H. Seager, D.R. Tallant, J.A. Voigt, B.E. Gnade, J. Appl. Phys. 79 (1996) 7983.
[31] D.C. Reynolds, D.C. Look, B. Jogai, H. Morkoc, Solid State Commun. 101 (1997) 643.
[32] C.M. Mo, Y.H. Li, Y.S. Lin, Y. Zhang, L.P. Zhang, J. Appl. Phys. 83 (1998) 4389.
[33] M. Liu, A.H. Kitai, P. Mascher, J. Lumin. 54 (1992) 35.
[34] L.E. Greene, M. Law, J. Goldberger, F. Kim, J.C. Johnson, Y. Zhang, R.J. Saykally, P. Yang, Angew. Chem., Int. Ed. 42 (2003) 3031.
[35] X.L. Wu, G.G. Siu, C.L. Fu, H.C. Ong, Appl. Phys. Lett. 78 (2001) 2285.
[36] S.A. Studenikin, N. Golego, M. Cocivera, J. Appl. Phys. 84 (1998) 2287.